Energy and AI 14 (2023) 100300

Contents lists available at ScienceDirect

Energy and AI

journal homepage: www.sciencedirect.com/journal/energy-and-ai

Mapping of decentralised photovoltaic and solar thermal systems by remote sensing aerial imagery and deep machine learning for statistic generation

Johan Lindahl [a,*], Robert Johansson [a], David Lingfors [b]

[a] Becquerel Sweden AB, SE-741 42 Knivsta, Sweden
[b] Department of Engineering Sciences, Uppsala University, SE-751 21 Uppsala, Sweden

HIGHLIGHTS

- High resolution statistics can be generated through remote sensing aerial imagery.
- Successive generation of training data and re-training improves the accuracy.
- An accurate ground truth makes it possible to quantify undetected solar systems.
- Frameless modules on dark roofs tend to be harder to detect.

GRAPHICAL ABSTRACT

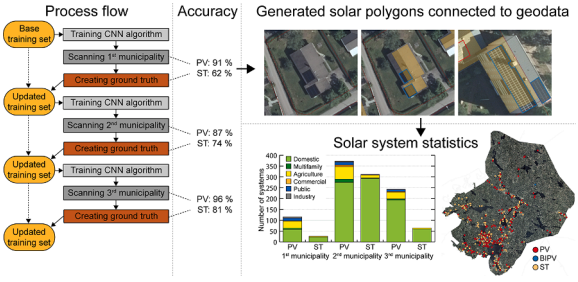

ARTICLE INFO

Keywords:
Photovoltaics
Solar thermal
Aerial imagery
Remote sensing
Object recognition
Convolutional neural networks

ABSTRACT

As a mean to monitor the rapid expansion of the highly decentralized PV market, identifying solar energy systems in aerial imagery by deep machine learning, is a research field that is getting increasing interest. One general challenge in the field is to create testing data of high quality that are representative of the end-use application. In this study we use the open source convolutional neural network developed within the DeepSolar project and apply it in the country of Sweden, for the purpose of generating market statistics, by scanning three complete municipalities for small decentralized photovoltaic and solar thermal systems. The evaluation of the performance is done against a highly accurate ground truth, which was created by cross-checking the classification results with the inventory of the local distribution system operators and the database of photovoltaic systems that have received a capital subsidy in Sweden, and combining that with physical onsite inspections. A process of generate additional training data and re-training the algorithm after each municipality scan was developed, which successively improved the accuracy, resulting in that 95% of all detectable photovoltaic, excluding building integrated and vertical systems, and 80% of all detectable solar thermal systems were correctly identified in the last municipality scan. The accurate ground truth allowed a quantification of why some systems are not detected. The generated dataset of solar energy systems could be connected to existing building and property inventories, which allowed creation of market segment statistics with remarkably high detail information.

* Corresponding author.
E-mail address: johan@becquerelsweden.se (J. Lindahl).

https://doi.org/10.1016/j.egyai.2023.100300

Available online 12 September 2023

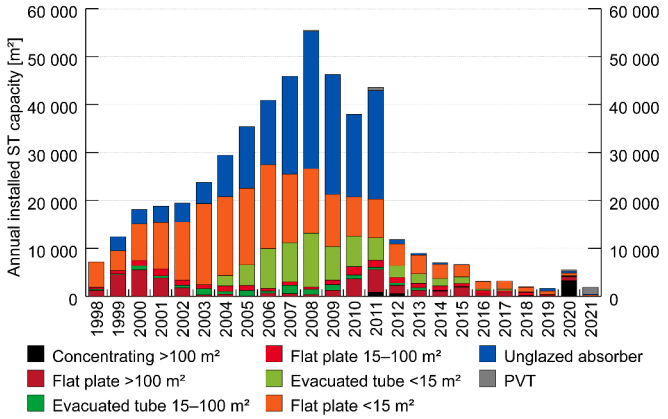

Fig. 1. Annual installed ST capacity in square meters based on voluntary sales statistics collected by Research Institutes of Sweden AB (RISE).

Abbreviations

BIPV	Building Integrated Photovoltaics
CNN	Convolutional Neural Network
DSO	Distribution System Operator
PV	Photovoltaics
SES	Solar Energy System
ST	Solar Thermal

1. Introduction

The conversion of the solar radiation to energy forms usable by the human society is increasing. Heating of buildings globally amounts to 260 300 TWh, which represents about 50% of global final energy use, of which 407 TWh was supplied by solar thermal (ST) applications in 2020 [1]. However, the global photovoltaic (PV) market is currently growing faster than the ST market [2], and has generally outpaced expectations over the past decade [3–5]. PV power production contributed to about 997 TWh in 2020, which corresponds to approximately 4% of the global electricity demand [2].

The scalable, low complexity and modular characteristics of the solar energy systems (SES) technologies lead to lower absolute unit costs and investment risks [6], which has made it possible for a large range of stakeholders to purchase, install and use the PV or ST technologies worldwide. Small-scale ST systems for direct heating of buildings or facilities represent about 60% of the installations [1] and likewise the PV market is made up of about 40% distributed systems [2].

The vast range in systems sizes and applications makes it hard for stakeholders to track the historical ST and PV deployment, and thereby accurately monitor the development on a global scale. The International Energy Agency Photovoltaic Power System Programme (IEA PVPS) has compiled information about how the registration of stationary PV systems is handled in several countries and suggests that countries should operate a compulsory database of PV power systems [7]. The recommendation is that such a database should cover all systems, not just those that receive different types of subsidies. However, in some countries that have implemented registration databases, small systems may legally be grid connected with no registration (or not reinforced), meaning there may be no official documentation of their existence [7–10]. In addition, the administrative capacity to follow the installation of PV systems is lacking in most countries. To expect all countries to implement and manage such a database as suggested by the IEA PVPS within the foreseeable future is unrealistic. The significant number of PV systems that have been [2], and will be installed [3,11,12], put pressure on public authority monitoring. The global ST market is also projected to grow in the coming years [13], but not at the same accelerated pace as the PV market. Hence, it is important to develop other methods to assess PV installation volumes.

A potential option to manually register stationary PV systems, which is gaining increasing interest in the scientific literature, is to identify PV systems and estimate their size, through remote sensing aerial imagery from satellites or planes and deep machine learning [14]. It has been proven that it is possible to generate databases of PV systems with exact location [10,15–24] and type of buildings [10,15,24] or land [17,25] used for the PV installations by this methodology, and combine these databases with socio-economic data for demographic investigations [15, 23,24]. Furthermore, this method has the potential to find off-grid and behind-the-meter PV installations that are either not registered or poorly visible to distribution system operators (DSO) [10]. However, PV systems need to be visible from the sky and have the clear characteristics of regular modules to be registered by this method, which means that vertical or high-tilted systems along with building integrated PV (BIPV) will not be identified. So far, most studies investigating this option have been focusing on generation of training images [26,27] or method development and validation [16,18,19,25,28–32], rather than statistic generation. However, three projects have used this approach to generate PV system inventories; the DeepSolar project, which detected 1.47 million PV systems across the US [15] and the DeepSolar++ model which produced a spatiotemporal dataset of 383 727 installations with installation year in the US [23], the inventory of [17], which mapped 68 661 commercial-, industrial- and utility-scale PV installations globally by remote sensing imagery between June 2016 and September 2018, and the Netherlands' Cadastre (Land Registry and Mapping Agency) that detected 156 637 buildings with PV in the three regions in the Netherlands. In addition, [21,22] combined neural network classification in aerial images and 3D building data to generate location, capacity, tilt and azimuth for existing PV systems and compared the result with the official German PV registry with more than one million buildings, and [20] evaluated the accuracy of mapping PV systems through aerial imagery and estimating their installed capacity as compared to a likewise imperfect dataset if 33 114 PV installations in the state of Connecticut, US.

In this study we address the issue of identifying small decentralized grid-connected and off-grid PV, along with ST systems, by aerial imagery and deep machine learning for statistic generation. We use the publicly available database and code from the convolutional neural network (CNN) DeepSolar framework [15] and apply it in the country of Sweden, which has a PV market with a relatively high number and share of stationary off-grid PV systems [33], small decentralized PV systems [34], and small-scale ST systems [35].

This study aims to make a contribution to the scientific community by assessing the real-world accuracy of identifying small decentralized PV and ST systems by a CNN aerial image classification algorithm by using aerial imagery of a combined area of 3 513 km^2 across three Swedish municipalities. While previous assessments of this kind have been conducted at a comprehensive level in the US [19], the Netherlands [10], and Germany [21], this research extends the scope by evaluating the algorithm's practical utility as an inventory tool and a statistical method for enhancing solar energy market development analyses. Additionally, the study establishes a highly accurate ground truth dataset, enabling a detailed quantification of the factors contributing to the non-detection of certain PV systems, an aspect that has not been extensively analysed before. Notably, the use of aerial imagery and deep machine learning to identify and separate ST from PV systems has to our knowledge only been done by [23]. By addressing these research gaps, the goal of this study is to advance our understanding of the potential and limitations of utilizing deep learning and aerial imagery in solar energy market assessments.

2. Background

2.1. The Swedish solar thermal market

In Sweden, the interest in ST has varied over the last decades, where

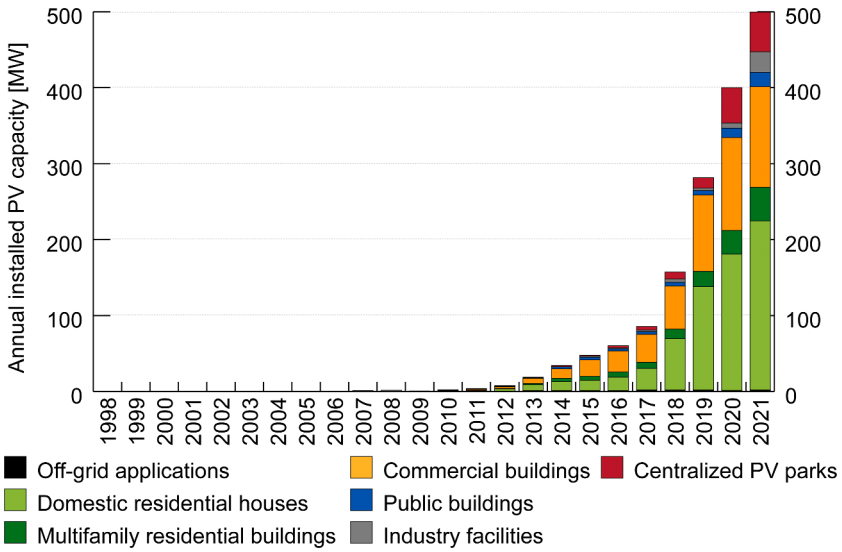

Fig. 2. Annual installed PV capacity in MW [33] based on statistics from Statistics Sweden for grid-connected systems, and sales statistics for off-grid and estimations regarding marked segments done within the Swedish IEA PVPS task 1 work.

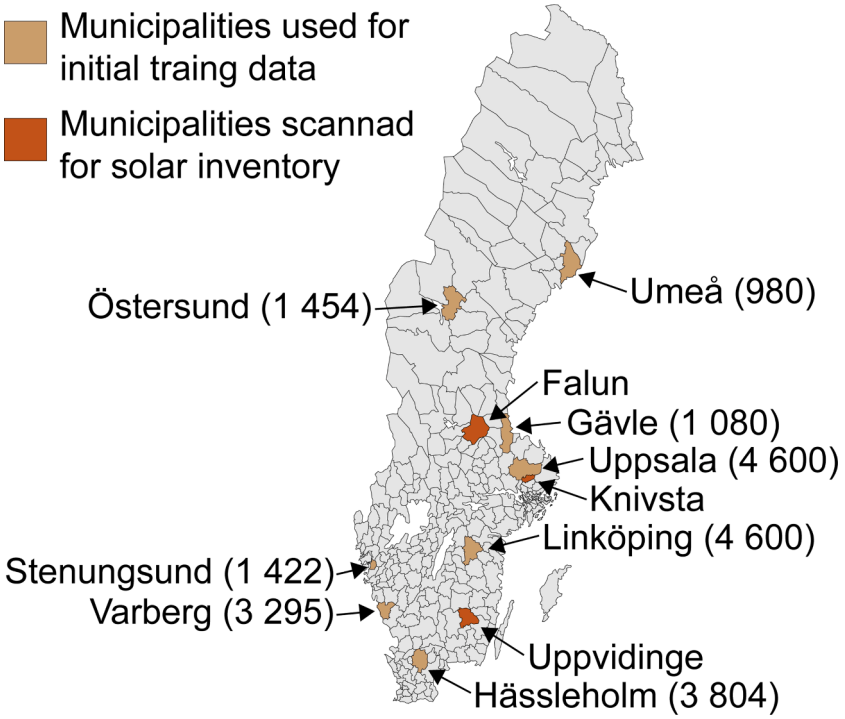

Fig. 3. The municipalities (yellow) used to draw initial training data from, with the number of image tiles from each municipality in parenthesis, and the three municipalities (red) that were scanned fully to create a solar inventory.

small-scale decentralized systems of less than 15 m^2 have largely driven the Swedish market, as shown in Fig. 1. Just like in the general situation in Europe [1], unglazed absorbers and flat plate collector systems account for the largest shares in Sweden.

Between 2000 and 2011, an investment subsidy for private individuals and small-scale systems was in place in Sweden [36], and a majority of the current Swedish ST systems were installed in that period. In 2011, the investment subsidies for ST were phased out after a total of 88 million SEK had been distributed, of which 98% was paid to single-family homeowners [36]. The Swedish ST market has since then declined, as Fig. 1 illustrates, as ST systems have had difficulty being profitable enough to be attractive with pure market conditions [35], which are in line with findings about the economics of unsubsidised ST in other European countries at the time [37].

Today, there is no direct support system for ST in Sweden. However, the installation costs for the ST systems are entitled to the Swedish ROT[1] tax deduction. The annual additions of ST systems are therefore small and are assessed through sales surveys sent to the ST installation firms,

[1] ROT is a collective term for measures to renovate and upgrade existing buildings owned by private individuals. The ROT-tax deduction in 2021 was 30 % of the labour cost and of maximum 50 000 SEK for the installation of a SES. The requirements are that the house is older than five years.

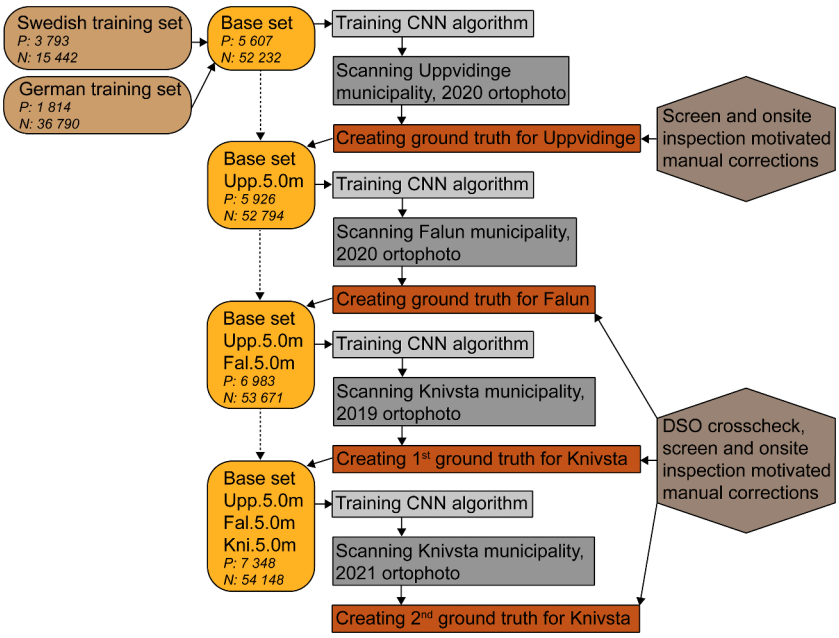

Fig. 4. Schematic illustration of the workflow of this study to create the SES database, with PV and ST systems from three municipalities. The letter P in the training set boxes stands for number of positive images and N stands for number of negative images.

with no geographical resolution at all. Just as in most other countries, ST systems are not registered by any Swedish authority and the knowledge of the market is therefore poor. It is assumed that most of the ST systems from the golden years of 2000–2011 remain up and running. However, their technical lifetime is coming closer to an end, so it would be beneficial to find ways to assess the decommission rate of ST systems in Sweden.

2.2. The solar photovoltaic market in Sweden

Historically, the Swedish PV market almost exclusively consisted of a small but stable off-grid market where the majority constituted of systems for holiday cottages, marine applications and caravans. The installation of grid-connected PV systems in Sweden can be said to have taken off in 2006 when about 300 kW was installed [33], and since 2007 more grid-connected PV capacity than off-grid capacity has been installed annually. The grid-connected market is to a large extent made up of distributed roof-mounted systems installed by individual homeowners, companies, municipalities, farmers, etc, see Fig. 2, and the dominating business model is to sell turnkey PV systems to these property owners [38]. So far only 8% of the grid-connected capacity is represented by ground-mounted centralized PV parks [33,39].

Already from the start, the Swedish market for distributed PV has been driven by self-consumption, as there has never existed a feed-in tariff in Sweden [33]. Capital subsidies in combination with a feed-in premium scheme, that add value for the excess electricity, have until now been crucial for this business model to work in Sweden. The Swedish capital subsidy programme was active between 2009 and 2021 in its latest form. Prior to that, there was support for energy efficiency in public premises, where PV was included as an eligible investment that could be applied for. The capital subsidy programme has been modified several times and the support level has been decreased as the market grew and prices fell. From 2009 to the end of 2021 a total of 3 545 million SEK has been disbursed [33]. However, as of 2022 no subsidies exist except for the private domestic PV market segment.

It is mandatory to notify the DSO when a PV system is connected to the grid. It is usually the AC power limit of the inverter, as this sets the limit of the power that can be fed into the grid, along with the commission date that is registered, but some grid operators also register the DC power of the system. Therefore, a DSO should have all the grid-connected PV systems within their grid area registered, and they are obliged to share the accumulated power with a geographical resolution on a municipality level with the Swedish Energy Agency once per year. Hence, no national database of all PV systems exists in Sweden.

3. Methodology and data

The work in this study is based on the classification branch of the open-access CNN DeepSolar framework [15], which identifies PV systems in aerial images. A slightly modified version of this CNN classification algorithm was used to scan the whole spatial area of the three Swedish municipalities; Uppvidinge, Falun and Knivsta (shown in Fig. 3). In this study, Python has been used as the programming language and QGIS as the programme for analysing the gathered and created geodata.

Fig. 4 illustrates the general workflow to create data sets of PV and ST systems for each municipality. In the following sections, the steps in this workflow are explained in detail. Section 3.1 describes the data sources. Section 3.2 describes the creation of a Swedish basic training set and how that is combined with an open-access training set from Germany. Section 3.3 describes the CNN classification algorithm. Section 3.4 defines the procedure to create a ground truth dataset for each municipality and the corresponding polygon layer shape file. Section 3.5 list the methods used to evaluate the results from the procedure of scanning municipalities. Section 3.6 describes how additional training data was gathered from each scanned municipality.

3.1. Data

Orthophotos provided by the Swedish Land Survey (Lantmäteriet) were used as the aerial images. Each orthophoto cover 2.5 × 2.5 km, which corresponds to 15 625 × 15 625 pixels, i.e., an original resolution of 0.16 m/pixel. A detailed description of the orthophotos is found in Appendix A. For the classification, the images are upsampled from tiles of size 115 × 115 pixels to 299 × 299 to match the DeepSolar format. The spatial resolution of the upsampled images is thus 0.0615 m/pixel. The aerial images of Uppvidinge in 2020 were taken either 2020-05-31 or 2020-06-01, of Falun in 2020 were taken either 2020-05-21, 2020-06-

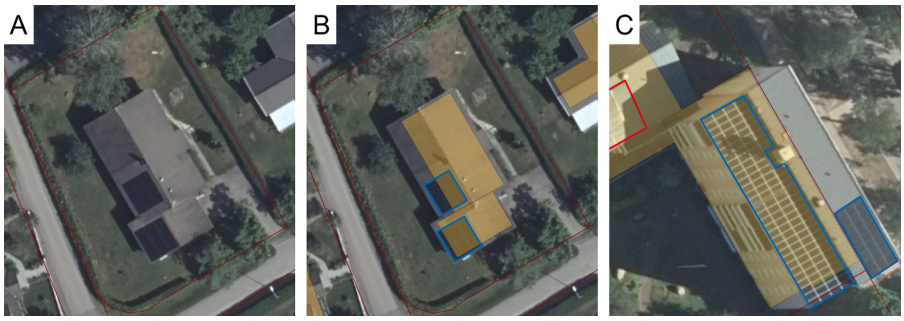

Fig. 5. Examples of identified PV (blue) or ST (red) systems in the Swedish Land Survey product Ortho-photo ©. In (a) PV modules installed on a detached residential house main building and adjacent garage with AY- Polygon layer from the Swedish Land Survey marking the boundaries of the property shown with a thin dark red line. (b) Same PV system and building, but with the BY- Polygon layer from the Swedish Land Survey marked with semi-transparent yellow shapes on top of the aerial imagery. (c) One ST and one PV system on two different multi-family houses within the same property.

11 or 2020-06-14, of Knivsta in 2019 were taken either 2019-07-19 or 2019-07-20 and the aerial images of Knivsta in 2021 were taken either 2021-04-16 or 2021-04-18.

For statistical classification of the SES's, official classification registries with standard definitions of both real properties and buildings are used. Firstly, the Swedish Tax Agencys (Skatteverket) classifies the purpose of all real properties for property taxation in a three-digit type code. See Appendix A, for a detailed description of the eight main categories.

Secondly, the Swedish Land Survey offers different geodata products. In this study we use; (1) "AY — Polygon layer with real properties and joint properties" and (2) "BY — Polygon layer with buildings", which are described in detail in Appendix A with the whole list of codes, purposes and descriptions.

3.2. Initial training dataset creation

Two different data sets were combined to train the CNN classification algorithm before the first complete scan of a municipality was conducted. Firstly, the open access data set called *OpenNRW_train_16* from [29] was used, which is a data set from North-Rhine Westphalia state in Germany containing 1 814 positive and 36 790 negative image tiles, with an upsampled resolution of 0.05 m/pixel.

Secondly, a Swedish set of images was created for fine-tuning [19] the DeepSolar CNN classification algorithm for Swedish conditions. This set was generated by using the database of the Swedish capital subsidy programme to locate properties that have received support for PV installation. This was done in eight municipalities from different parts of the country, see Fig. 3. Then orthophoto image tiles overlapping these properties were extracted and manually labelled as "positive" if they contained a PV system or "negative" if not. This was done following a similar approach suggested by [18,26,29] with two annotators (engineering students) going through all image tiles. If both annotators agreed on an image tile it was labelled accordingly. In cases there was a disagreement between the two annotators, a third annotator (the main author of the study) made the final judgement if the image tile was positive or negative, which took place for about 0.5% of the images. The number of image tiles from each municipality is listed in parentheses in Fig. 3. In total 3 793 positive and 15 442 negative image tiles were generated this way, which should be noted only refers to PV systems. For the record, the mean *solar panel proportion distribution* [40] was found to be lower in the Swedish training set compared to the German. No training set for ST systems could be created in a similarly efficient way, as there does not exist any register of ST systems in Sweden.

The images of the German *OpenNRW_train_16* set were scaled down from 320 × 320 pixels to 299 × 299 pixels, so that the sizes of the image tiles had the same size as the Swedish ones. For comparison, the resolution of the German image tiles is 0.0545 m/pixel and the Swedish 0.0615 m/pixel. These two data sets were combined for training the CNN classification algorithm, and we refer to this combined training set as the *base set* in the rest of the article. The base set, hence, contains 5 607 positive and 52 232 negative image tiles in total.

3.3. The CNN classification algorithm

The CNN classification algorithm is the one described in [15], but modified to run using Pytorch[2]. Of the three pytorch models available from the papers [29] and [21] we choose the file called *DeepSolar_GoogleMaps_classification.tar* as a starting point, as training that model with our *base set* gave better results on a test set consisting of 2000 images from Sweden. The training was done for 100 epochs and all layers of the model were set as trainable. The imbalance rate (the weight given to the rarer samples in the loss function) was set to five, as this setup was considered the best after an iterative value analysis.

3.4. Creation of a ground truth

The initial step in creating a "ground truth" for a municipality is scanning all the orthophotos for that municipality using the CNN classification algorithm. All orthophoto tiles classified to contain a SES were added to a shape file. This shape file in combination with data from the Swedish capital subsidy programme, in which each property that has received support is registered, was used as a support for manually identifying SESs in the municipalities. The location and the system boundaries of the identified PV and ST systems were marked by creating polygon objects in a separate shape file. In addition, the polygon object was manually assigned the technology, i.e., if was a ST or PV system. Through the polygon object, the identified systems were assigned coordinates and a 2-dimension area extent seen from above. Examples of identified solar thermal and PV systems are illustrated in Fig. 5.

By the AY polygon layer, illustrated by the thin dark red lines in Fig. 5, the *property designation* (real estate boundary) can be assigned to the solar energy polygon objects. Similarly, the BY polygon layer is used to appoint the SES polygon objects the *detailed purpose* code of the building it is installed on. The BY polygon layer is shown as a yellow-semi-transparent area in Fig. 5b and c.

Some SESs are ground mounted. In this study, a SES is assigned the detailed purpose of the closest BY polygon layer object if it is found within 5 meters (in the real world) and is given the detailed purpose "ground" if the SES polygon object is >5 meters from the closest BY polygon layer object. The reason for this approach is the shift artefact that sometimes occurs between the BY polygon layer as compared to the orthophoto, which arises for tall buildings when the aerial image was not taken directly from above (previously discussed by [10]). Such a shift is illustrated in Fig. 5c, where one side (with balconies) of a tall multi-family house can be seen in the image. In some cases where this method gives the wrong result, the solar system polygon objects have been corrected and assigned the proper building manually.

The property designation is the identification key used to connect the identified PV systems to the information that exists for individual PV systems in the local DSO's databases. The identified PV systems were

[2] The code can be downloaded from https://github.com/wangzhechen g/deepsolar_pytorch.

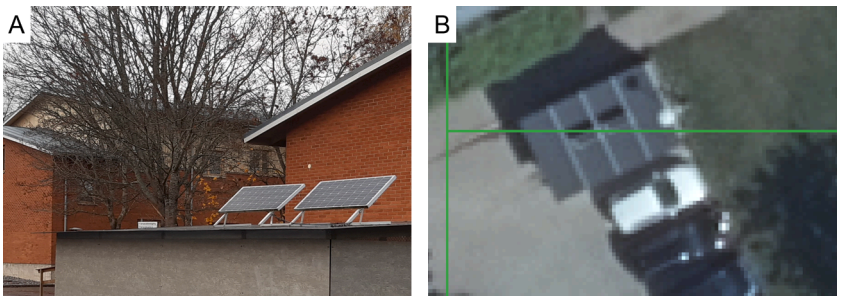

Fig. 6. An off-grid PV system on a small garbage collecting building containing two PV modules. (A) A regular photo of the system. (B) The corresponding orthophoto ©, from the Swedish Land Survey, of the system, and the two image tiles overlapping the system.

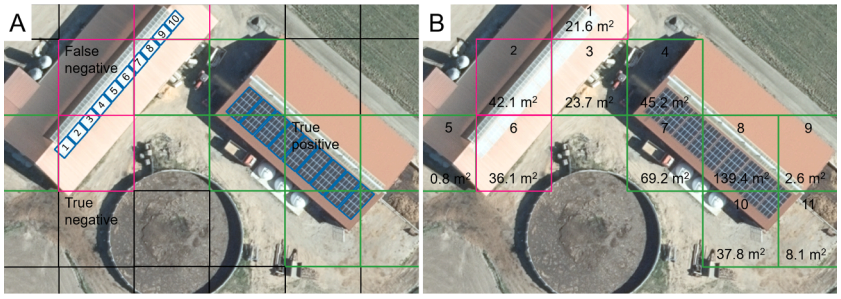

Fig. 7. PV polygons (blue-framed in A) on two barns containing several sets of PV modules with spaces in between each set, in a orthophoto © from the Swedish Land Survey. (A) Examples of true positive image tiles (green), false negatives (magenta) and true negatives (black), along with ten PV polygon objects on the left barn and nine PV polygon objects on the right barn. (B) The positive image tiles are numbered at the top of each square and the total area of the PV polygon objects in each of the positive image tiles is listed at the bottom.

crosschecked with the two local DSOs internal databases in the municipalities of Falun and Knivsta. Unfortunately, this was not possible for the Uppvidinge municipality, as the local DSO believed that this would contravene their internal juridical arrangement. Through the crosscheck procedure, some systems could be corrected in terms of technology, and PV systems that were not detected could be identified and added as polygon objects by looking in the aerial imagery at the property designation where the DSO had registered a PV system that was not found by the CNN classification algorithm.

The lack of a registry of ST systems, made it impossible to crosscheck the identified ST systems in the same way as was done for PV systems. However, ST systems manually detected in the aerial imagery, but not identified by the CNN classification algorithm were also added as polygon objects.

In a last step, physical on-site inspection was conducted to verify the existence of an SES, or the type of technology (PV or ST), in case of uncertainty in all of the three municipalities, and the polygon objects of SESs were corrected in some cases. The final shape files containing added and corrected polygon objects of PV and ST systems are hereafter referred to as the "ground truth".

3.5. Evaluation methods

Accuracy analysis is important for deep learning model evaluation. As we in this study use a slightly modified version of the CNN DeepSolar framework, the same method as in [15,29] is used for evaluating the classification, i.e., using metrics based on true/false positives/negatives, where a true positive (TP) corresponds to the CNN finding an actual SES within an image tile.

From the total number of TP, false positives (FP), true negatives (TN) and false negatives (FN) we evaluate our model runs for each municipality in terms of the precision, sometimes also referred to as "correctness", which is defined as;

$$precision = \frac{TP}{TP + FP} \tag{1}$$

and the recall, sometimes called "completeness", which is defined as;

$$recall = \frac{TP}{TP + FN} \tag{2}$$

Precision measures the ratio of correct predictions among positive predictions, while recall measures the ratio of actual positive samples that can be identified [33]. In addition, also the F1 score is calculated [10,19,28], which is an overall measure of a model's accuracy defined by the harmonic mean of precision and recall;

$$F1 = 2 \times \frac{Precicion \times Recall}{Precicion + Recall} \tag{3}$$

However, as the image tiles that are evaluated at a municipality scan are positioned side by side in our setup, it is inevitable that some tiles only will consist of a very small area of a SES, i.e. a low *solar panel proportion*. Logically it is harder for the CNN classification algorithm to correctly identify a SES when only a small chard of a SES is in it. However, in some cases the CNN algorithm was shown to be capable of identifying small systems containing only one or two panels, for instance in Fig. 6b, the bottom image tile is only 0.7 m^2.

To deal with the uncertainty of images containing only very small parts of a SES, we define a category of image tiles as *borderline* tiles. These tiles represent all image tiles that only cover 0–0.5 m^2 of SES polygon objects from the ground truth dataset. Borderline image tiles are considered neither positive, as it in many cases would be unrealistic to expect the CNN classification algorithm to correctly identify a very small shard of a solar energy panel, nor negative, as they actually contain a part of a SES and therefore would be wrongly labelled if the CNN classification algorithm detected the shard of the SES. The borderline tiles are therefore removed from the total set of image tiles in the accuracy evaluation but are listed for reference.

Just as [10] points out, classification accuracy is the ratio of correct predictions to the total number of input samples, and as most image tiles dont contain a SES, high accuracy would be achieved if all tiles were classified as negative. So, in addition to the analysis of individual image tiles, a second approach based on object-wise metrics, which is preferable for counts of SES arrays [20], to evaluate the accuracy is proposed and used in this study. As the goal of this study is to evaluate the possibility to use CNN frameworks to generate solar energy statistics and to

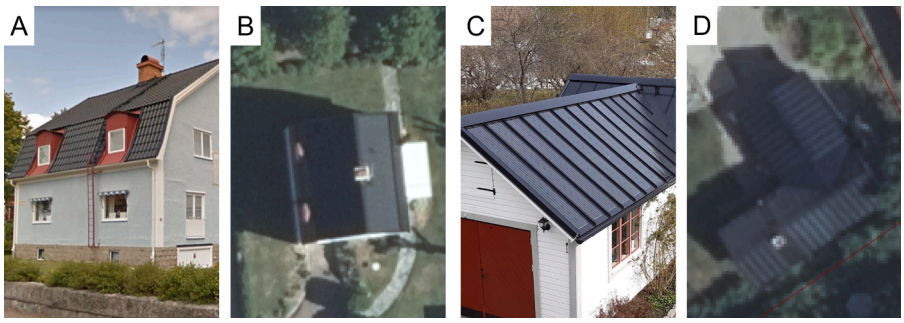

Fig. 8. Example of BIPV systems considered as undetectable by a remote sensing aerial imagery method. (A) A PV roof tile system from Rustabo AB and (B) the orthophoto © from the Swedish Land Survey of the same building. (C) A CIGS thin film seam metal roof from Midsummer AB and (D) the orthophoto © from the Swedish Land Survey of the same building.

use it as an inventory tool, it is of higher importance that at least one part of a SES is identified and not all parts of it. Fig. 7 illustrates such an example. In Fig. 7a, all six image tiles covering the PV polygon objects on the right barn were correctly classified as positive, i.e., TP, while three of the image tiles on the left barn were classified as negative by the CNN classification algorithm, i.e., FN. The PV polygon objects in Fig. 7a marked 1, 7, 8 and 9 are partly covered with an image tile that the CNN classification algorithm has labelled as positive. A polygon object that is fully or partly overlapped by one or several true positive image tiles, like the mentioned example, is defined as a "detected polygon".

We define a system as a group of solar panels located on the same building. If any of the polygons on the building is overlapped by at least one true positive image tile, it is defined as a "detected system".

Furthermore, a property can contain several buildings with SESs on each of them. In Sweden the DSOs regard everything behind each grid connection point as one single electrical system, and properties usually only have one grid connection point each. So, in order to match this definition and compare the results to the registries of the DSOs, we create a third polygon group that contains all solar energy polygon objects within a property. Likewise, if such a property polygon group is overlapped by one or several true positive image tiles, it is defined as a "detected property".

The *detected polygon* object-wise metric is compared to the total number of polygon objects in the ground truth of a municipality, while *detected system* and *detected property* are compared to the total number of buildings and properties, respectively, in a municipality that according to the ground truth dataset contained a SES.

3.6. Generating additional training data

After the creation of the ground truth for a municipality, additional training data can be generated from that municipality, as all image tiles covering the municipality have been labelled either TP, TN, FP or FN. Since a class imbalance situation for data, where PV panels make up a small part of the whole image, poses a challenge for the training of deep learning models [40], one need to find the right balance on how large of an area of a solar system that a positive image tile should contain for it to be a good sample to train the CNN classification algorithm on. Therefore, an investigation was performed after the first municipality scan of Uppvidinge, which used the *base set* training data. The investigation was performed on the second municipality (Falun) in which the CNN classification algorithm was trained with the *base set* plus complementary image tiles from Uppvidinge. Based on the ground truth polygon layer of Uppvidinge municipality, positive training samples were defined as image tiles that contained at least an area X = [0.5, 2.5, 5, 7.5 m^2] of a part, but not the entire, solar energy polygon. However, in case an image tile contained the entire solar system polygon object, the limit of at least 0.5 m^2 (see Section 3.5) was kept in all of the runs. The negative samples added for the additional training were all the FP image tiles from Uppvidinge. Hence, since X was varied, the number of positives varied in each training set used for the four scans of Falun. To concretize this in an example it would have meant that all eleven positive (green) image tiles in Fig. 7b would have been used as positive training samples if X = 0.5 m^2. If X = 2.5 m^2, image tile 5 would have been left out for the training, and if X = 5 m^2 also tile 9 would have been omitted. The four additional training sets from Uppvidinge are denoted *Upp.0.5m, Upp.2.5m, Upp.5.0m* and *Upp.7.5m*, respectively.

4. Results

The result of the evaluation of the CNN classification algorithm capability as means of generating statistics about the PV market is presented in this part. Firstly, Section 4.1 discuss the definition of undetectable SESs and Section 4.2 the main reasons why some SESs are not detected by the CNN classification algorithm. Then follows the evaluation of the CNN classification algorithm and generation of additional training data analysis in Section 4.3 based on the metrics of precision, recall, detected polygon, detected system and detected property. Section 4.4 describes some positive aspects of scanning a municipality a second time. Lastly, Section 4.5 concludes the generation of a statistical data set from this method.

4.1. Undetectable solar energy systems

Following the scanning of the municipalities, and then manually crosschecking with the local DSO, it was concluded that some PV systems were not detected. Some of these PV systems can be sorted into two categories that we in this study regard as *undetectable* by remote sensing aerial imagery methods. These two categories are building integrated PV (BIPV) and vertically installed PV modules. BIPV cells/modules are designed to blend into the built environment and the buildings they are installed on. That characteristic makes it very hard or impossible to identify that it is PV from long distances, especially from an aerial image, as Fig. 8 illustrates. Likewise, vertically installed PV modules cannot be detected in an image that is taken from above. These two types of systems could only be identified through the cross-checking with the DSOs databases and onsite inspections. Missing BIPV and vertical systems is an obvious drawback of the approach of statistic generation through classification through aerial images. However, through the cross-check with the local DSOs and physical inspections in the municipalities of Falun and Knivsta, only 10 BIPV systems, 5 vertical grid connected PV systems, and 2 vertical ST systems were identified, which means that the number of BIPV and vertical SESs were few compared to regular building applied (BAPV) roof mounted SESs in these two municipalities. The identified BIPV and vertical PV systems were added to the SES polygon layers of the different municipalities and the generated data base of SESs, but were omitted for the generation of additional training data and considered as negative image tiles in evaluations of the CNN classification algorithm presented in the next section.

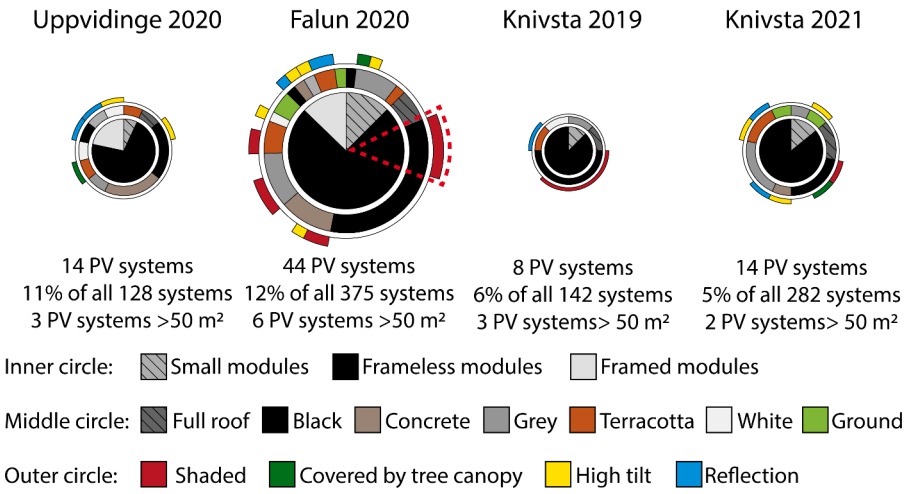

Fig. 9. Summary of the underlying factors that are common for undetected PV systems. The size of the circle diagrams represents the number of undetected PV systems in each municipality. Each pie piece of the inner circle charts represents a certain number of PV systems that share the module characteristics. These systems are also in the graph geometrically connected to the roof colour characteristics in the middle circle and some common aggravating characteristics in the outer circle. As an example, the red dashed pie piece represents five undetected PV systems made up of frameless modules, installed on a black roof and that was shaded in the aerial image used to create the orthophoto.

Table 1
Accuracy evaluation of the different municipality scans based on the stated training datasets and performed in the workflow order illustrated by Fig. 4, which mean from left column to right column in the table.

	Technology	Uppvidinge 2020	Falun 2020					Knivsta 2019		Knivsta 2021	
Training dataset		Base	Base	Base Upp.0.5m	Base Upp.2.5m	Base Upp.5.0m	Base Upp.7.5m	Base	Base Upp.5.0m Fal.5.0m	Base	Base Upp.5.0m Fal.5.0m Kni.5.0m
Total # image tiles	-	3 645 323	6 767 141	6 767 141	6 767 141	6 767 141	6 767 141	877 142	877 142	877 142	877 142
# Borderline	-	31	108	108	108	108	108	32	32	56	56
# True Positive	Both	267	944	931	936	934	940	353	359	601	625
	PV	248	677	675	667	674	672	305	301	558	569
	ST	19	281	270	283	274	282	51	61	46	60
# False Positive	-	562	1 582	1 268	1 501	877	862	647	474	601	353
# True Negative	-	3 644 353	6 764 126	6 764 440	6 764 207	6 764 831	6 764 846	876 003	876 176	875 706	875 954
# False Negative	Both	110	381	394	389	391	385	107	101	178	154
	PV	93	222	224	232	225	227	67	71	138	127
	ST	17	161	172	159	168	160	40	30	41	27
Precision	Both	32.2%	37.4%	42.3%	38.4%	51.6%	52.2%	35.3%	43.1%	50.0%	63.9%
Recall	Both	70.8%	71.2%	70.3%	70.6%	70.5%	70.9%	76.7%	78.0%	77.2%	80.2%
	PV	72.7%	75.3%	75.1%	74.2%	75.0%	74.7%	82.0%	80.9%	80.2%	81.8%
	ST	52.8%	63.6%	61.1%	64.0%	62.0%	63.8%	56.0%	67.0%	52.9%	69.0%
F1	Both	44.3%	49.0%	52.8%	49.8%	59.6%	60.1%	48.4%	55.5%	60.7%	71.1%

4.2. Undetected solar energy systems

The PV systems that were not detected by the CNN classification algorithm were investigated closer, based on the *detected system* definition, to see if those had some common characteristics. Firstly, they were divided into three types of module characteristics; (1) *Small modules* — modules that in the orthophoto appeared to be significantly smaller than normal-sized modules (in almost all cases these were used in stationary off-grid systems), (2) *Frameless modules* — modules that do not have a characteristic frame, and (3) *Framed modules* — modules with a distinctive frame, traditionally made of aluminum.

Secondly, we classified the colour of the roof into six general traditional roof colours, and a seventh category if it was ground mounted. These were; (1) *Full roof* — which is when the PV modules completely cover a full geometric part of the roof so that the material beneath are not visible, (2) *Black* — black coloured roofs, (3) *Concrete* — a brownish grey colour that is typical for concrete tiles, (4) *Grey* — different shades of grey, which includes roofs which appear to be made of steel or aluminum roof sheets, (5) *Terracotta* — the colour of traditional brick pans, (6) *White* — white or very light grey appearing roofs, and (7) *Ground* — for ground mounted PV systems.

In addition, four other common aggravating characteristics for the undetected PV systems were identified in the analysis, which were; (1) *Shaded* — the whole, or a part, of the PV system was shaded by surrounding trees, buildings or part of the same building it was installed on, (2) *Covered by tree canopy* — whole, or a part, of the PV system is covered by a tree canopy in the orthophoto, (3) *High tilt* — modules that have been installed with a high tilt, usually >45°, which makes them appear with different (often skewed) dimensions in the orthophotos, as compared to systems installed with a lower tilt, and (4) *Reflection* — modules that appear bright white due to the angle between the sun, their orientation and the camera, causing a strong reflection when the aerial image is taken.

All undetected PV systems were classified with one of the three module characteristics and one of the seven roofs (and ground) appearances, along with the aggravating characteristics if present. Qualitatively, we present examples of different undetected PV systems according to this classification in Appendix B. Quantitatively, the result of this classification exercise is presented in Fig. 9.

The general conclusion from Fig. 9 is that small modules, regardless of the colour of the roof, give rise to a number of undetected PV systems. Furthermore, *frameless* modules, together with either a *black* or *full roof*

Table 2
Accuracy comparison of studies that include detection of decentralised PV systems in the built environment, along with information on image resolution and the data sets evaluated.

Study	Model	Country	Precision [%]	Recall [%]	F1 [%]	Image resolution [m/pixel]	Number of images evaluated	Share of positive samples of the images [%]
[18]	ConvNet	US (1)	81.2 / 85.5	84.0 / 87.3	82.6 / 86.4	0.30	-	-
[19]	SolarMapper	US	0.76	0.77	0.76	0.30	-	-
[15]	DeepSolar	US (3)	93.1 / 93.7	88.5 / 90.5	90.7 / 92.1	0.15	93 500	1.31
[29]	DeepSolar	US	91.0	98.1	94.4	0.05	3 798	4.08
[10]	TernausNet	the Netherlands	93.1	90.7	91.9	0.10	2 791 904 (3)	5.61
[21,22]	DeepSolar	Germany	87.3	87.5	87.4	0.10	45 060	0.85
This study	*DeepSolar — CNN*	*Germany*	*93.4*	*81.3*	*86.9*	*0.10*	*45 060*	*0.85*
This study	**DeepSolar — CNN**	**Sweden**	**63.9**	**81.8**	**71.1**	**0.16**	**877 142**	**0.09**

(1) In Boston respective San Francisco
(3) In residential respective non-residential areas
(3) Number of buildings and not images

setup give rise to a majority of the undetected PV systems. In addition, *frameless* modules on roofs with a distinctly different roof colour, such as concrete, grey, terracotta or white, usually are combined with one of the four aggravating characteristics if they are undetected, most commonly when they are *shaded*. Lastly, for the *framed* modules, which logically should be the easiest for the CNN classification algorithm to detect due to the distinctive frame, which sets each module apart from its neighbour module and the roof, the *shaded, high tilt* or *reflection* characteristics are present in almost all cases of undetected systems.

In addition to the appearance of the systems summarized in Fig. 9, it was also noted that smaller PV systems are slightly overrepresented as undetected, which are in line with the problems arising from low solar panel proportion distribution [40]. Of systems with an area corresponding to >50 m^2 in the orthophotos, only 4% were undetected in Uppvidinge, 4% in Falun, 5% in the 2019 Knivsta scan and 2% in the 2021 Knivsta scan, which can be compared to the overall undetection rate of 11% in Uppvidinge, 12% in Falun, 6% in the 2019 Knivsta scan and 5% in the 2021 Knivsta scan.

For the undetected ST systems, no analysis was conducted as a clear trend of an improved detection rate can be read from the Tables 1 and 3, as a consequence of added training data over ST systems after each municipality scan, and we therefore believe that the major reason for undetected ST systems still is a lack of training images for ST systems.

4.3. Evaluation of the CNN classification algorithm

Each municipality scan was analysed based on the parameters described in Section 3.5, and the results are presented in Table 1. As described in Section 3.4, our created solar energy polygon layer contains information on whether a polygon object is a PV or ST system. This allows for splitting up the number of TP image tiles and FN image tiles into the two technologies PV or ST. It should be noted that the sum of the number of TPs for PV and ST, respectively, in Table 1, does not add up to the stated number of total TP image tiles for both technologies for Falun and Knivsta. The reason is that, for these municipalities, there were 14, 3 and 4 image tiles, respectively, that overlapped with both a PV and a ST polygon and thus included as TP for both PV and ST in Table 1. The same goes for FN in Falun, where two image tiles that overlap with both a PV and a ST polygon were not found in any of the four different scans.

The four scans on the Falun municipality, based on the *base set* plus each of the training setups from Uppvidinge, see Section 3.6, were evaluated against the created ground truth of Falun by calculating the precision, the recall and the F1 value. The results are shown in Table 1, and as can be seen the number of FP image tiles dropped significantly between the scan where the CNN classification algorithm had been trained with the *base set* plus *Upp.2.5m*, and the scan based on the *base set* plus *Upp.5.0m*, while there was only marginal changes in the number of TP image tiles. Hence, an improvement in precision from 38.4% to 51.6%, while negligible influence on recall, was achieved when the minimum limit of 5.0 m^2 was implemented for the generation of additional training data as compared to the limit of 2.5 m^2. The number of FP image tiles deceased only slightly when the minimum threshold was set to 7.5 m^2. The result is logical, as the number of additional training image tiles decreased when the minimum threshold is increased (e.g., from 377 to 341 positive images between the *Upp.2.5m* and *Upp.5.0m*), while a too low threshold led to that unsuitable image tiles were included in the training. We therefore used a setup for the scans of Knivsta municipality where positive training samples are generated from earlier municipality scans if an image tile contains an entire solar energy polygon object of at least 0.5 m^2, or if a tile overlaps with at least 5.0 m^2 of parts of one or several solar energy polygon objects, as this seems to lead to good results while still generating a larger number of training images as compared to if the 7.5 m^2 threshold is used. The used additional training data added after each municipality scan are accordingly denoted *Upp.5.0m, Fal.5.0m*, and *Kni.5.0m,* respectively.

As both the number of TP and FP image tiles can be assigned to either of the two technologies, the recall for each technology can be calculated. As can be seen in Table 1, the recall for PV is higher than the recall for ST in all scans. This is an expected result, as there was no efficient way of generating training data over ST systems beforehand, which lead to that the *base set* do not contain any image tiles of ST systems. But after each municipality scan, the recall for ST increases significantly, which is attributed to training images tiles over ST systems being added in the generated additional training sets after each municipality scan.

The precision accuracy evaluation can, on the contrary, not be calculated for the two individual technologies separately, since FP image tiles cannot be attributed to either the ST or PV technology, and consequently the F1 value can only be calculated for both technologies together.

In general, it is concluded that the approach of extracting additional training data after each municipality scan and re-training the CNN algorithm with the images (some of which it previously got wrong) successively improves the accuracy, as compared to the scans where only the base set have been used for the training. As Table 1 illustrates, the absolute change in precision were an increase of 13.9 percentage points, while the recall for both technologies and the F1 score was improved by 3.1 percentage points and 10.5 percentage points, respectively, in the last scan of Knivsta.

Even if the focus on this paper is the practical process of generating statistics, it is of interest to compare the accuracy of this study with

Table 3
Accuracy evaluation by the object-wise metrics found polygon, found system and found property compared to the ground truth of the different municipality scans based on the stated training datasets and performed in the workflow order illustrated by Fig. 4, which mean from left column to right column in the table.

		Uppvidinge 2020		Falun 2020		Knivsta 2019		Knivsta 2021	
Technology		PV	ST	PV	ST	PV	ST	PV	ST
Polygon	Ground truth	238	30	849	373	282	77	562	77
	Found	216	18	756	271	271	60	533	62
	Share	91%	60%	89%	73%	96%	78%	95%	81%
System	Ground truth	128	27	375	313	142	67	282	66
	Found	114	16	328	231	134	52	268	53
	Share	89%	59%	87%	74%	94%	78%	95%	80%
Property	Ground truth	116	26	329	312	124	65	240	64
	Found	105	16	285	231	120	51	230	52
	Share	91%	62%	87%	74%	97%	78%	96%	81%

Fig. 10. Orthophotos © from the Swedish Land Survey over PV systems in Knivsta. (A) Same property as in Fig. 5a, where an additional set of PV modules have been installed on the northern part of the roof. (B) Building with a PV system which was not identified by the CNN classification algorithm in the scan of the orthophoto from 2019. (C) The same building and PV system as in (B), but in the orthophoto from 2021, which was correctly classified as a PV system by the CNN classification algorithm in the second scan.

previous studies. Some of the previous studies have focused on detecting large PV parks, like [16,17,25,30,31], which is a different matter compared to small decentralized PV systems. However, the studies based on the DeepSolar project [15,21,22,29], along with [10,18,19] all focus on decentralized PV in the built environment. The accuracies achieved in these studies are presented in Table 2, along with our result for the last scan in this study (Knivsta 2021) in bold. In addition, we ran the CNN algorithm, trained the same way as in the last municipality scan (*Base set* + *Upp.5.0m* + *Fal.5.0m* + *Kni.5.0m*), on the *OpenNRW_Test_16* test set of [29] for comparison, and the results are presented in the second last row in italic in Table 2. Even if the distribution shift [14,20] caused by differences in geography and type of images should be kept in mind, it is worth noting that the addition of the training data from Sweden seems to have improved precision as compared to the results of [21,22].

As a remark, it can be perceived that the second scan of Knivsta is biased, as we have generated positive training image tiles over 209 (those systems that existed in July 2019) of the total 348 SESs that CNN classification algorithm is intended to locate. However, as the aerial images of 2021, as compared to those of 2019, are taken at different time of the year (July vs. April), time of the day and different solar intensity, several aspects of the images of the same objects differ between the two scans. For example, this includes how the shadows fall, perceived colours of both SESs and buildings, leafing of threes and moving of non-stationary objects or changes of buildings. Due to these changes in the imagery, which are traditional aspects in distribution shifts (or domain gaps) that give rise to worse performance when applying a classification algorithm to a new location [14,19,20], and where especially lighting conditions results in heterogeneous colour features [40], we claim that an eventual bias is negligible.

Regarding the three object-wise metrics, the results are listed in Table 3. Just as for precision and recall, the share of *detected polygon, detected system* and *detected property* are for every scan higher for PV than for ST, which is due to the same reasons as discussed previously. However, the share of found ST systems is increasing steadily when the CNN classification algorithm is gradually trained with progressively more image tiles showing ST systems. In the end, 95% respective 80% of all detectable PV respective ST systems where found in the 2021 scan of Knivsta. This is for at least the PV systems a high enough number for the method to be used to generate databases for statistical purposes. It should be noted, that these numbers do not include 'undetectable' BIPV and vertical PV systems, that to our knowledge were two of each in Knivsta.

4.4. Second scan of Knivsta

For the first scan of Knivsta, orthophotos from 2019 were used, and the aerial images had been taken at either 2019-07-19 or 2019-07-20. For the second model run of Knivsta, the aerial images taken in 2021, at either 2021-06-18, 2021-06-21, or 2021-08-28, were explored. This allows studying the changes in the fleet of SESs between mid-2019 and mid-2021. As expected, the number of PV systems increased significantly (see Table 3), following the national trend (see Fig. 2) and confirms that identifying SES in aerial images by deep machine learning is a tool that can be used to analyse PV adoption trajectories [23] and track the market development with a high spatial resolution.

One special case of the additional deployment is the property shown in Fig. 5a, that added another set of modules, which can be seen in Fig. 10a. This type of expansion of capacity within a property is something that the DSO is not always aware of in Sweden, as reporting to the DSO only is mandatory when a property first adds the capacity to produce electricity or when the fuse of the property is changed. We noted 2 such expansions of PV systems in Knivsta between the two aerial image scans performed in this study. In addition, in the comparison with the local DSO database, we found 2 earlier presumable PV system capacity expansions in Knivsta and 1 in Falun, that seem to have taken place before the aerial images were taken.

Additionally, the second scan of Knivsta allowed for identification of SESs that were decommissioned between the two setups of aerial images. Comparing the ground truth results of the second scan of Knivsta with the first scan revealed that 2 ST systems had been dismantled during the period.

We also observed that 7 of the 8 PV systems, and 8 of the 15 ST systems, that were not detected by the CNN classification algorithm in the first scan of Knivsta were correctly classified in the second scan. This can probably partly be explained by the adding of training data from the

Table 4
Statistical summary of the building and property purposes based on the detected property metric of the PV systems in the ground truth dataset for the three scanned municipalities.

General building purpose	Detailed building purpose	Property purpose	Number of systems			
			Uppvid-inge 2020	Falun 2020	Knivsta 2019	Knivsta 2021
Ground	-	Single-family dwelling units				2
		Agriculture units		2	1	1
Residential	Small house, detached	Single-family dwelling units	27	199	74	159
		Tenement building units	1			
		Agriculture units	6	11		
		Industrial premises units		1		
		Special units		1		
	Small house, chain linked house	Single-family dwelling units		18	4	7
	Single family houses, terraced houses	Single-family dwelling units		2	1	3
		Tenement building units			1	1
	Small house with several apartments	Tenement building units		1		
	Multi-family house	Tenement building units	3	12	3	3
		Single-family dwelling units	1			
		Special units	1			1
	Unspecified	Single-family dwelling units	3			
		Agriculture units	1	1		
Complementary	Unspecified	Single-family dwelling units	20	41	13	22
		Tenement building units	1	2		
		Agriculture units	31	47	18	25
		Industrial premises units	2	2		
		Power-generation units	1			
		Special units	3			1
Agricultural	Unspecified	Single-family dwelling units		2		1
		Agriculture units		3		3
Industrial	Wood industry	Industrial premises units	1			
	Other manufacturing industry	Tenement building units	1	1		1
	Other industrial building	Industrial premises units	1			
	Unspecified	Industrial premises units	1	1	1	1
		Single-family dwelling units		1		
Public	School	Special units		5	3	4
	Higher education institution	Industrial premises units		1		
	Hospital	Special units		2		
	Healthcare centre	Tenement building units	1			
	Fire station	Special units		1		
	Town hall	Special units		1		
	Cultural building	Special units	1			
	Associations	Tenement building units		1		
	Sports hall	Special units			1	1
	Ice rink	Industrial premises units	1			
		Special units	1			
	Public baths	Special units	1			
	Riding stables	Agriculture units			1	1
		Special units	1			
	Unspecified	Special units	2		1	1
		Tenement building units	1	1		
Activity	Unspecified	Single-family dwelling units		1		
		Tenement building units		2		1
		Industrial premises units	2	5	1	2
		Special units		1		
Other building	Unspecified	Single-family dwelling units		1		
		Tenement building units			1	1
		Agriculture units			1	1
Total			116	370	125	243

Table 5
Statistical summary of the building and property purposes based on the detected property metric of the ST systems in the ground truth dataset for the three scanned municipalities.

General building purpose	Detailed building purpose	Property purpose	Number of systems			
			Uppvid-inge 2020	Falun 2020	Knivsta 2019	Knivsta 2021
Ground	-	Single-family dwelling units			2	2
	-	Agriculture units		1		
Residential	Small house, detached	Single-family dwelling units	14	196	38	36
		Tenement building units		1		
		Agriculture units	3	36	7	8
		Power-generation units		1		
	Small house, chain linked house	Single-family dwelling units		9		
	Multi-family house	Tenement building units		3		
	Unspecified	Single-family dwelling units			2	2
		Agriculture units	2			
Complementary	Unspecified	Single-family dwelling units	5	50	11	11
		Agriculture units	2	11	5	5
	Other industrial building	Industrial premises units		1		
Public	School	Special units		1		
	Sports hall	Special units		1		
Activity	Unspecified	Tenement building units		1		
Total			26	312	65	64

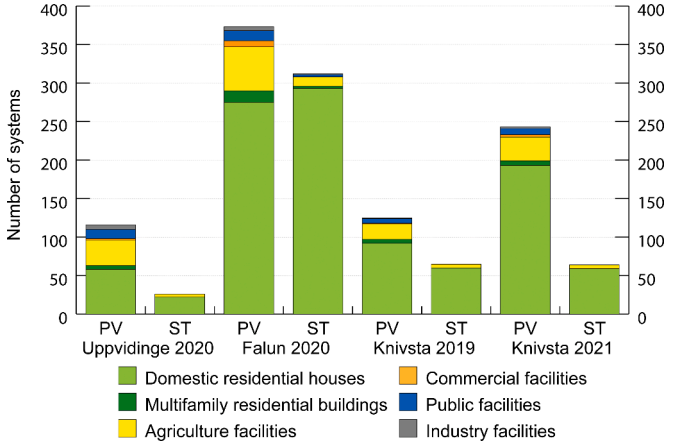

Fig. 11. Summary of number of PV respective ST systems in the ground truth of the three municipalities.

first scan, which includes image tiles of these missing system, and partly by changed conditions in the orthophotos due to the difference in time stamps. Fig. 10 b and c illustrates an example of the later, where a PV system was in a complete shadow in the orthophoto from 2019-07-19 (foliated trees at time of aerial image), which led to it not being correctly classified by the CNN classification algorithm, but well visible in the orthophoto from the aerial image taken 2021-04-16 (due to defoliated trees at the time of this aerial image), and by that correctly identified.

To summarize, continuous scans of a municipality on regular basis will disclose changes in the fleet of SESs, both newly installed systems and dismantled systems, as well as the chance of revealing previously unidentified system.

4.5. Statistical generation

So far, evaluations of the accuracy of the CNN classification algorithm and the results in terms of practically building a database of decentralised SESs have been addressed. Lastly, this section summarizes what type of statistics that is possible to extract with this method. First, the obvious conclusion is that the spatial resolution of this method is very high. SESs can be allocated with an exact coordinate and an area spread seen from above. This allows to assign them to specific buildings (or the location on the ground). This is a higher resolution than what most of the Swedish DSOs have, as they are only notified that there exists a PV system with a certain capacity behind a certain grid point, which is usually equivalent to that they know that a PV system exists within a certain property. For the ST technology, only aggregated sales statistics

Table 6
The number, general purpose of the property and the definition of type codes for property taxation in Sweden.

The tax agency's type code	Type of taxation units	Prescribed combination of buildings and land
100 series	Agriculture units	Economy building, arable land, pastureland, productive forest land and forest impediment. Also detached houses and land for detached houses located on agricultural property.
200 series	Single-family dwelling units	Detached houses and plots of land for such buildings.
300 series	Tenement building units	Tenements apartment buildings and plots of land for such buildings.
400 series	Industrial premises units	Industrial buildings, other buildings, land for such buildings as well as certain waterworks and fishing properties.
500 series	Owner occupied flats units	Condominiums and plot of land for such buildings
600 series	Quarries	Extension land as well as industrial buildings and other buildings on such land.
700 series	Power-generation units	Power plant building, land for power plant building and taxation unit whose value predominantly consists of the right to share- or replacement power.
800 series	Special units	Special buildings and plot of land for such buildings.

Table 7
Code list for building purposes and detailed purposes of the BY - Polygon layer with buildings.

Code	Purpose of building	Detailed purpose	Description
130	Residential	Small house, detached	Small house with a dwelling that is not connected to another small house
131	Residential	Small house, chain linked house	Two or more single family houses joined via a garage, storeroom or similar. Each home is on private property; semi-detached houses are also classified as chain linked houses.
132	Residential	Single family houses, terraced houses	Small houses in a row of at least three houses whose dwelling parts are directly joined with each other and where each dwelling is on private property.
133	Residential	Multi-family house	Building with at least three dwellings. May sometimes contain an office, shop, hotel, restaurant or similar. At least 50% must be residential.
135	Residential	Small house with several apartments	Small house with several apartments that are on the same property. E.g., two residential houses, rental or tenant-owned, with at least three apartments.
199	Residential	Unspecified	Home with unknown residential purposes. Stated only by Lantmäteriet when using updating methods that cannot determine the purpose.
240	Industrial	Other manufacturing industry	Building for other industrial activities involving manufacturing.
241	Industrial	Gas turbine plant	Facilities for production of electricity using combustion gases.
242	Industrial	Industry hotel	Building that contains several different industries. E.g., industrial building.
243	Industrial	Chemical industry	Industry for the manufacture or processing of chemical products. E.g., paint industry, plastics industry, pharmaceuticals industry.
244	Industrial	Condensing power plant	Facilities for the production of electricity from steam; does not utilise waste heat.
245	Industrial	Nuclear power station	Facilities for the production of electricity from nuclear energy.
246	Industrial	Food industry	Industry for the production of food, by the processing of agricultural products among other things. E.g., processed meats, canning industry, fruit industry.
247	Industrial	Metal or machinery industry	Industry for the production and processing of metals and machinery. E.g., car industry, iron works, mechanical industry, metal industry, shipbuilding.
248	Industrial	Textile industry	Industry that manufactures yarn, cloth etc. and prepares these. E. g., textile and clothing, weaving.
249	Industrial	Wood industry	Industries for processing wood raw materials. E.g., wood, pulp and paper and furniture industries, paper mill, sawmill, carpentry.
250	Industrial	Hydro power facilities	Facility that converts potential energy of water into electricity.
251	Industrial	Wind turbine	Facility for the conversion of wind energy into electricity.
252	Industrial	Heat plant	Facility that delivers district heating from boilers that burn solid, liquid or gaseous fuels and consume electricity. E.g., combined heat and power facilities or district heating facilities.
253	Industrial	Other industrial building	Other building for industrial activities (possibly without walls) not involving manufacturing, e.g., warehouse, petrol station, repair workshop.
299	Industrial	Unspecified	Industry with unknown purpose.
301	Public	Public baths	Building with public bathing facilities. E.g., public baths, open-air swimming-bath, swimming pool, adventure pool.
302	Public	Fire station	Building for rescue services.
303	Public	Bus station	Large bus stop or travel centre with several lines with buildings. E.g., travel centre.
304	Public	Distribution building	Building for distribution networks for gas, heating, electricity or water. E.g., transformer station, district heating plant, cabinet (telecommunications, broadband), water tower, grid station.
305	Public	Animal hospital	Building for stationary care of sick animals.
306	Public	Defence building	Building used for defence purposes or defence preparedness. E.g., building adjacent to a military establishment or military store.
307	Public	Healthcare centre	Unit for non-hospital care. E.g., healthcare centre, care centre, medical care centre, open care centre. Not private surgery, however.
308	Public	Higher education institution	Post-secondary school classified as higher education institution.
309	Public	Ice rink	Built-in artificially frozen ice facility. E.g., for ice hockey, bandy or ice skating.
310	Public	Railway station	Station or stop that expedites passenger or goods traffic under SJ provisions (SJF 611) and the national timetable.
311	Public	Town hall	The main building for municipal management. E.g., government offices, town hall, civic centre.
312	Public	Prison	Institution for the enforcement of custodial sentences, e.g., penitentiary institution or prison.
313	Public	Cultural building	Building used for cultural purposes. E.g., theatre, museum or local history museum.
314	Public	Police station	Building used as a centre for police operations.
315	Public	Sewage treatment plant	Building for the treatment of wastewater.
316	Public	Riding stables	Building with manège for horse riding, e.g., riding stables, riding school.
317	Public	Associations	Building for established organised religious association. E.g., church, non-conformist church, mosque, synagogue, temple, monastery, parish house, crematorium, chapel or burial chapel.

(continued on next page)

Table 7 (*continued*)

Code	Purpose of building	Detailed purpose	Description
318	Public	Hospital	Establishment for inpatient care and specialised outpatient care. E.g., hospital, county hospital, regional hospital.
319	Public	School	Building for education. E.g., preschool, compulsory school, upper secondary school, school for people, trade, hunting, agriculture, nature and culture, natural resources, nomads, rescue, forestry, engineering, healthcare or Sami.
320	Public	Sports hall	Indoor sports facility for sports such as badminton, curling, tennis.
321	Public	University	Higher education classified in the Higher Education Ordinance.
322	Public	Waterworks	Facility where groundwater or surface water is purified into drinking water. For example, water purification facilities.
324	Public	Multi arena	Flexible large arena for sports, cultural and other types of events.
399	Public	Unspecified	Public function with unknown purpose.
499	Activity	Unspecified	Public function with unknown purpose.
599	Agricultural	Unspecified	Agricultural building with unknown purpose.
699	Complementary	Unspecified	Complementary building with unknown purpose.
799	Other building	Unspecified	Other building with unknown purpose.

on a national level exist in Sweden, so the spatial resolution of this methodology far exceeds the current Swedish ST statistics.

Furthermore, as described in Section 3.4, the possibility to allocate the identified SESs to certain buildings and properties makes it possible to assign them the general building purpose, the detailed building purpose and the property purpose. The results of the taxonomy of all the SESs, on the *property* metric level in the ground truth, are presented in Table 4 for PV and in Table 5 for ST. For instance, the largest number of both PV and ST systems are found on the building types *Residential; Small house, detached* and *Complementary; Unspecified*. The purpose of the former is straight forward, and these installations belong to the market segment usually referred to as "private residential" or as we use to define it "Domestic residential houses". However, the latter building category can represent many different types of buildings, as this can both be for example garages (Fig. 5b), which naturally should be part of the private residential market segment, or barns (Fig. 7), which rather belong to an agriculture market segment. However, a clear indication of what type of complementary building it is can be received with the additional information about the property purpose from the Swedish Tax Agency.

As Tables 4 and 5 illustrates, a very high resolution on 'market segments' can be achieved, at least in Sweden, by implementing a method of identifying SESs by aerial imagery and deep machine learning. The resolution is so high in Tables 4 and 5 that it is hard to get an overview. Hence, by combining the detailed purpose of buildings and the property purpose we group the rows in Tables 4 and 5, by the colour code seen in these tables, into six more classical defined market segments that we call (1) Domestic residential houses — light green, (2) "Multifamily residential buildings" — dark green, (3) "Agriculture buildings" — yellow, (4) "Commercial buildings" — orange, (5) "Industry buildings" — grey, and (6) "Public buildings" — blue. The results of this exercise are presented in Fig. 11, which clearly shows that, when it comes to the number of SESs, a clear majority are installed within the domestic residential houses market segment in these three municipalities. It should be noted that several off-grid systems are included in these numbers. Second most common are the agriculture market segment and third commercial facilities. This is an interesting observation, as it has not been possible to separate these two market segments from each other in the existing statistical databases in Sweden until now. Hence, the commercial market segment in Fig. 2 includes both agriculture and commercial facilities. Public facilities and industry facilities stand for only a few PV and ST system in each municipality, but each such system is in general much larger than the systems for domestic residential houses, so in terms of capacity they would stand for larger market shares.

5. Discussion

The focus of this paper has not been on improving the CNN algorithm or methodology to reach the highest possible accuracy, but rather proposing a method to scan large regions with the purpose of setting up databases of SESs for inventory and statistical purposes. Currently, our process contains two manual steps that should be possible to automate. The first is the creation of a polygon to represent the area spread of the identified SESs. This step could be advantageously replaced by an automatic artificial neural network segmentation model, and within the current research project a U-net model, similar to those implemented by [10,16,17,28,30] for segmentation is developed and evaluated [41].

Secondly, the classification of the solar energy technology, i.e., PV or ST, have been executed manually in this study. The main reason for that was the lack of training data for the ST technology. We had no efficient way to generate training images over ST systems in Sweden. However, from the four municipality scans in this study a total of 656 image tiles over ST systems are now labelled. If more municipalities are scanned in the same manner, the number of labelled ST images will increase, and they should eventually amount to enough images for training the model to automatically differentiate the two technologies from each other.

The lower accuracy achieved in this study as compared to some previous work, see Table 2, can be explained by several factors. One obvious factor is the resolution of the imagery, as high resolution is needed to reliably evaluate fine-grain features such as SES panels. Table 2 include information about the imagery resolution of the different studies for comparison.

Regarding the lower precision achieved in this study as compared to the previous publications, one explanation is that our scans of complete municipalities in the sparsely populated Sweden contain a much larger share of negative images than the mentioned studies. As Table 2 show, the share of positive image tiles is lower, with factors of ~10 to ~500, in the municipality scans of this study as compared to the test sets in the previous studies. A larger share of negative image tiles will naturally generate relatively more FP images as compared to TP images, resulting in a worse precision by definition. This explanation is to a large extent confirmed as we achieved a precision of 93.4%, as compared to 63.9%, when we ran the equally trained CNN algorithm on the *Open-NRW_Test_16* test set of [29], which has an almost ×10 higher share of positive images.

Regarding the recall, our number of 81.8% are lower as compared to previous studies, but not as far below as the precision. As the main goal is to evaluate how useful detection of decentralised of SES's by aerial images and a CNN classification algorithm are for creating as comprehensive a database as possible, a high recall is more important than a high precision, as the recall measures the ratio of actual positive samples that can be identified.

One reason for our slightly lower recall values could be that we have a more accurate ground truth than most previous studies. To our understanding, all of the studies in Table 2 Table 1 used manual annotations to create the ground truth, and only [21,22] compared their results with known PV locations from PV registries (registries with substantial errors in them [20,21]). As a notable exemption from the lack of comparison with an existing database, [21] state that 16 out of the 160 PV systems above 30kW$_p$ in the German 'Marktstammdatenregister' in their

investigated area were not detected in the classification step, and that they found 21 PV systems that are not listed in the official registry. As a comparison, we found in Knivsta and Falun in total 5 PV grid-connected PV systems that were either missing or not correctly registered in the DSO database, 47 additional off-grid systems that by definition the DSO do no records of and 1 grid-connected PV system that had been dismantled without reporting to the DSO.

Consequently, it is likely that some very difficult cases (like frameless modules on black roof with for example either a high tilt, shadows or reflections) are not correctly annotated as positive in the previous studies that we in Table 2 compare our results with. Subsequently, the typical assumption that the ground truth is infallible is unlikely correct in these studies, as the error rate of the annotators is unknowable without known locations to compare with [20]. For example, it takes a very skilled or lucky person to detect the PV system in Fig. 10b or for some of the examples in Appendix B. In [20], they estimate that the annotators missed about 3.8% of the visible panels, and 5.0% if also non-visible systems were included. As we had two different registers to cross-check our result for detecting PV systems against, and also conducted on-site inspections in some cases, our ground truth is probably more reliable than in any of the previous studies in the field, and consequently contain several positive image tiles that it is very difficult for a person (or a CNN classification algorithm) to detect.

A way of improving the process used in this paper, and possibly the accuracy, could be to implement a mosaicking with sliding windows approach, like [30] did with improved result when the stride value was decreased. Mosaicking results in overlapping image tiles, which would make it possible to increase the *solar panel proportion distribution* [40], and thereby exclude what we defined as borderline image tiles from the analysis without any loss of information or investigated area. However, such an approach would increase the computational cost [30], which, depending on the used striding value, could limit the practicality to scan large regions, like municipalities.

Another way to improve the accuracy could be to implement pre-processing steps, such as only scan images that overlap buildings, or post-processing steps, like [10] that deleted all results that covered greenhouses. Only evaluating images covering buildings would have had a positive effect on the accuracy, as many FP image tiles in the first scans covered land features such as symmetrically ploughed fields, roads, lakes with waves and power lines. However, such a measure would make it impossible to identify the 8 ground-mounted SESs detected in the three municipalities, and hence would have resulted in lower accuracy in our object-wise metrics. Opposite to the Netherlands, which host a lot of greenhouses [10], we found no specific building that often led to FP classification. A potential post-processing step that would have improved the accuracy in Sweden could instead be to remove FP on clearly north-facing roofs.

Lastly, since the CNN algorithm detected 67% of the ST systems in the first municipality scan, even if no image of a ST system (intentionally) was included in the training, we find it surprising that the visual resemblance (see Fig. B.7 in Appendix B) between the two SES technologies, PV and ST, are almost not discussed at all within the research field. The exemption is [23], that developed a multi-class CNN classification model that classify each SES into four subtypes, of which one is ST systems. Our results, and the lack of reflection upon the similarity of the two technologies in the literature, raises a perhaps uncomfortable, but springing question; How many of the perceived identified PV systems in previous studies are actually ST systems? This question is perhaps most relevant for small-scale decentralized SES classification and segmentation, as ST is usually mounted on roofs [1,42,43], but the ST technology can also be built in large scale (and be ground mounted) for district heating and industrial applications [44–46], and can consequently be confused for PV parks.

6. Conclusions

The study encompassed a comprehensive analysis of three Swedish municipalities using CNN classification algorithms applied to orthophotos, with the primary aim of identifying and categorizing PV and ST systems for statistical purposes. The iterative process involved multiple scans, with the CNN algorithm being retrained after each municipality scan, resulting in progressively enhanced accuracy. In the initial scan, the algorithm detected 89% of the detectable PV systems (excluding BIPV and vertical installations) and 59% of the ST systems. Remarkably, by the fourth and final scan, these detection rates improved to 95% for PV systems and 80% for ST systems. This accuracy underscores the model's ability as both an inventory tool and a mechanism for constructing comprehensive databases of existing SESs. Connecting such a database, where the exact locations of the SESs are known, to existing building and property inventories, facilitates the generation of remarkably detailed SES market segment statistics.

The process of SES classification, combined with cross-referencing against two distinct PV databases and on-site inspections, yielded a precise ground truth. This allowed for meticulous analysis and quantification of the attributes associated with undetected PV systems (false negatives), a dimension heretofore largely unexplored in existing literature. Conclusions drawn from this analysis indicated that frameless modules, typically installed on darker-coloured roofs, constituted the majority of undetected PV systems. Additionally, factors such as shading from trees or structures, image reflections, and systems with high tilt angles were identified as conditions that impeded the CNN classification algorithm's detection efficacy.

Notably, a subsequent scan of one municipality, conducted two years later demonstrated the dynamic nature of SES detection. The second scan revealed that most of the previously missed SESs, comprising 7 out of 8 PV systems and 8 out of 15 ST systems, were successfully identified. This finding underscored the impact of differing conditions at the time of aerial imagery acquisition. Moreover, the second scan illuminated the potential for aerial imagery and machine learning not only to track the commissioning of new SESs but also to monitor the decommissioning of old systems.

In summation, this research makes a contribution to the scientific landscape by addressing the real-world accuracy of CNN-based identification of decentralized PV and ST systems. Through systematic scans of three municipalities and the establishment of a precise ground truth, the study uncovers factors that impact detection rates, thereby advancing the practical application of deep learning and aerial imagery in solar energy market assessments.

Declaration of Competing Interest

The authors declare the following financial interests/personal relationships which may be considered as potential competing interests: Johan Lindahl reports financial support was provided by Swedish Energy Agency.

Data availability

The authors do not have permission to share data.

Acknowledgements

The authors gratefully acknowledge the financing from the Swedish Energy Agency (grant number P50265-1). The Swedish Energy Agency had no involvement or influence in any part in the study. In addition, the authors want to thank Nicholas Etherden at Vattenfall R&D (Vattenfall is the DSO in Knivsta) and Oscar Willén at Falu Energi & Vatten AB (the DSO of Falun) for their help with cross-checking our results against their databases.

Appendix A

Orthophoto

Orthophotos are radiometrically processed aerial photography data, geometrically projected to an orthogonal map projection by using an elevation model. In an orthophoto the scale or distance between points are not affected by variations in the terrain, which is the case in an aerial photo with central projection.

The product Orthophoto contains orthogonal projected aerial photos (orthophotos) with different combinations of wavelength bands and resolutions. Since 2019, orthophotos with a resolution of 0.1 m/pixel, and 4-channel (Red, green, blue, Infrared), exist for Sweden and it is these orthophotos that have been used in this project. The orthophotos are taken at a flight altitude of 3000 meter, and each orthophoto cover 2.5 × 2.5 km (15 625 × 15 625 pixels) with approximated horizontal standard errors of 0.2 m.

Photos taken before leafing do not contain that much IR-information. Therefore, the photos can be more or less suitable for different areas of application, depending on the time of photography. Other factors can also give some amount of variation in the photos. Examples of such factors are fog, sun angle and conditions on the ground, such as drought, at the time of photography. Especially the sun angle is of importance for this project as some PV system look like white/shining in the orthophotos when the angle of the sun and tilt and azimuth of the modules are in such position so that direct sunlight is reflected into the camera.

Depending on where in the aerial photo a building lies, i.e., how far away from a building the flight line is, more or less of the façade can be visible on the orthophoto. When a building lies in the middle of an aerial photo, the photo is taken directly above the building and then you only see the roof of the building and nothing of the façade. When a building lies far away from the flight line, i.e., near the edge of an aerial photo, you see the building obliquely from above, hence you can also see relatively much of the façade. So, depending on where in the aerial photo the building lies, more or less of the façade can be visible.

For this reason, differences may occur between different flight years, due to that the same area has been overflown with different flight lines and side coverage, so that on an orthophoto from a specific flight year the façade of a certain building might not be visible at all, while on an orthophoto from another flight year relatively much of the façade of the same building is visible.

The ambition is to photograph approximately 30 % of the country each year; more frequently and with higher resolution in densely built-up areas in the south of Sweden and along the coast of Norrland, but less frequently and with lower resolution in the inland of Norrland and in the northern mountain ranges.

Type codes for property taxation

During the property taxation, which takes place every three or six years, the Swedish Tax Agency determines a three-digit designation type code for each property which describes the purpose of the property. The type code is an administrative designation and is not based on any legal requirement according to law or other provision. How the properties are to be divided into different types are defined in chapter 4, Section 5 of the Property Taxation Act (SFS 1979:1152). In this study, we only use the first number in the three-digit designation type code, and the number, general purpose of the property and the definition of those are summarised in Table 6.

AY — Polygon layer with real properties and joint properties

The AY layer contains polygons for real properties and joint properties. Polygon creation takes place by municipality and comprehensive polygons are created. Quality controls are carried out to provide information on the polygons' structural quality. The AY polygons contain several types of information, and the important ones for this project is (1) County and municipality code and name, (2) District name, e.g., BERGA, and (3) Block and unit, e.g., 1:3. By combining the District name and Block and unit, the Property Designation is acquired. The Property Designation is the unique designation/name that each individual property has been given in Sweden.

BY — Polygon layer with buildings

The BY layer contains building geometries. Most of the buildings are measured by either the roof or façade edge of the building. All Swedish municipalities have signed a collaboration agreement with Lantmäteriet on updating buildings and all municipalities have building presentations. In addition to the position and the buildings measures the layer contains information about the purpose that a building is used for. These are (1) Residential — Building that is predominantly used for permanent or leisure accommodation, (2) Industry — Building that is predominantly used for the manufacture of products or processing of raw materials, (3) Public — Building that is predominantly used for citizens' activities in a public context, (4) Commercial — Building that is predominantly used for commercial purposes, (5) Agriculture — Building that is predominantly used for agricultural, forestry or comparable industry, (6) Complementary — Building belonging to other buildings with residential, social function, business or industrial purposes and (7) Other building — Building whose purpose is not Residential, Industrial, Social, Commercial, Agricultural or Complementary.

Detailed purposes are specified for buildings with the building purposes of Residential, Industrial and Public purpose, see Table 7 for the whole list and the codes. When a building has several different building purposes, such as residential and business, the building's main purpose is stated.

Appendix B

Examples of undetected PV systems and ST systems

Examples of different undetected PV systems according to the three classifications discussed in Section 4.2 are shown in the following Figs. B.1-B.6. Firstly, three types of module characteristics; (1) Small modules, (2) Frameless modules, and (3) Framed modules. Secondly, general traditional roof

colours (and ground mounted); (1) Full roof — which is when the PV modules completely cover a full geometric part of the roof so that the material beneath are not visible, (2) Black, (3) Concrete, (4) Grey, (5) Terracotta, (6) White, and (7) Ground. Thirdly, four common aggravating characteristics for undetected PV systems; (1) Shaded, (2) Covered by tree canopy, (3) High tilt, and (4) Reflection.

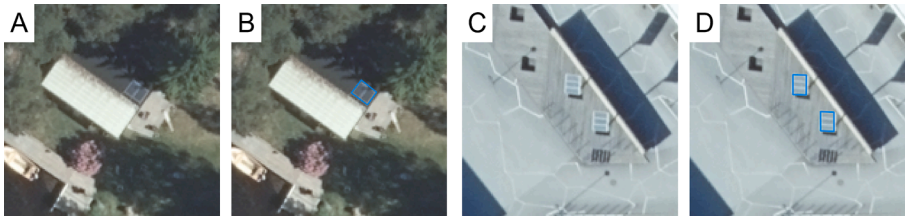

Fig. B.1. Orthophotos © from the Swedish Land over undetected PV system. (A) and (B), 'Small modules' on a 'Grey' roof and 'Hidden by tree canopy', with and without the manual created PV polygon, respectively. (C) and (D), 'Small modules' on 'Ground' with a 'Hight tilt', with and without the manual created PV polygons, respectively.

Fig. B.2. Orthophotos © from the Swedish Land over undetected PV system. (A) and (B), 'Framed modules' on a 'Terracotta' roof with 'Reflection', with and without the manual created PV polygon, respectively. (C) and (D), 'Frameless modules' on a 'Terracotta' roof with 'Reflection', with and without the manual created PV polygons, respectively.

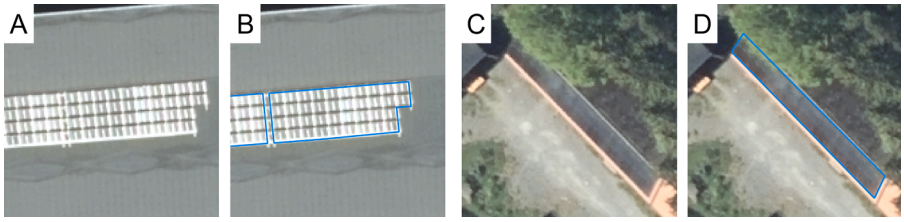

Fig. B.3. Orthophotos © from the Swedish Land over undetected PV system. (A) and (B), 'Framed modules' on a 'Grey' roof with 'Reflection', with and without the manual created PV polygons, respectively. (C) and (D), 'Frameless modules' on a 'Terracotta' roof and 'Hidden by tree canopy', with and without the manual created PV polygon, respectively.

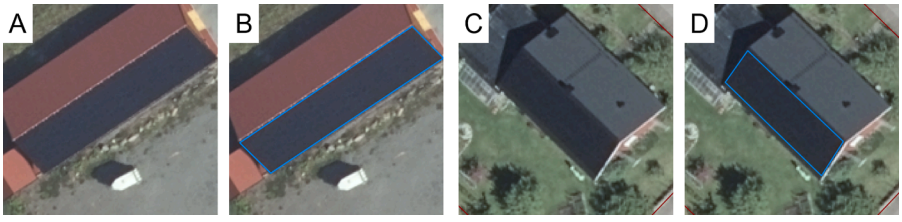

Fig. B.4. Orthophotos © from the Swedish Land over undetected PV system. (A) and (B), 'Framed modules' as a 'Full roof', with and without the manual created PV polygon, respectively. (C) and (D), 'Frameless modules' as a 'Full roof', with and without the manual created PV polygon, respectively.

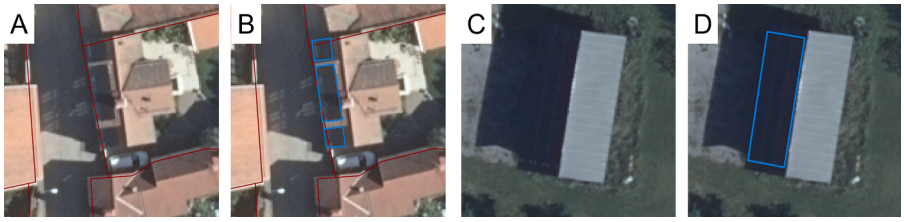

Fig. B.5. Orthophotos © from the Swedish Land over undetected PV system. (A) and (B), 'Frameless modules' on a 'Terracotta' roof that is 'Shaded', with and without the manual created PV polygons, respectively. (C) and (D), 'Frameless modules' on a 'Grey' roof that is 'Shaded', with and without the manual created PV polygon, respectively.

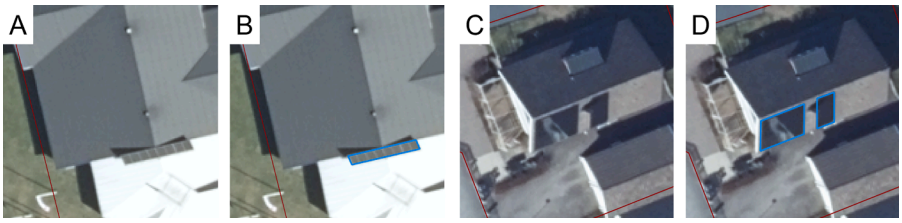

Fig. B.6. Orthophotos © from the Swedish Land over undetected PV system. (A) and (B), 'Framed modules' on a 'White' roof with a 'Hight tilt', with and without the manual created PV polygons, respectively. (C) and (D), 'Frameless modules' on a 'Concrete' roof with a 'Hight tilt', with and without the manual created PV polygons, respectively.

In addition, Fig. B.7 illustrates some different kind of ST systems, that could be mistaken for PV systems by a CNN classification algorithm.

Fig. B.7. Orthophotos © from the Swedish Land over undetected PV system. (A) An evacuated tube absorber ST system, (B) a roof integrated flat plate absorber ST system, (C) a roof applied flat plate absorber ST system, and (D), an unglazed absorber ST system.

References

[1] Weiss W, Spörk-Dür M. Solar heat worldwide — 2021 Edition. 2021.
[2] IEA PVPS task 1, Masson G, Kaizuka I, Bosch E, Plaza C, Scognamiglio A, et al. Trends in photovoltaic applications — 2022. 2022.
[3] Jaxa-Rozen M, Trutnevyte E. Sources of uncertainty in long-term global scenarios of solar photovoltaic technology. Nat Clim Chang 2021;11:266–73. https://doi.org/10.1038/s41558-021-00998-8.
[4] Victoria M, Haegel N, Peters IM, Sinton R, Jäger-Waldau A, del Cañizo C, et al. Solar photovoltaics is ready to power a sustainable future. Joule 2021;5:1041–56. https://doi.org/10.1016/j.joule.2021.03.005.
[5] Creutzig F, Agoston P, Goldschmidt JC, Luderer G, Nemet G, Pietzcker RC. The underestimated potential of solar energy to mitigate climate change. Nat Energy 2017;2. https://doi.org/10.1038/nenergy.2017.140.
[6] Wilson C, Grubler A, Bento N, Healey S, de Stercke S, Zimm C. Granular technologies to accelerate decarbonization. Science (1979) 2020;368:36–9.
[7] IEA PVPS, Fechner H, Johnston W, Neubourg G, Masson G, Ahm P, et al. Data model for PV systems — Data model and data acquisition for PV registration schemes and grid connection evaluations — Best practice and recommendations. 2020.
[8] Stowell D, Kelly J, Tanner D, Taylor J, Jones E, Geddes J, et al. A harmonised, high-coverage, open dataset of solar photovoltaic installations in the UK. Sci Data 2020;7:1–15. https://doi.org/10.1038/s41597-020-00739-0.
[9] Kasmi G, Dubus L, Blanc P, Saint-Drenan Y-M. Towards unsupervised assessment with open-source data of the accuracy of deep learning-based distributed PV mapping. Workshop on Machine Learning for Earth Observation (MACLEAN), in Conjunction with the ECML/PKDD 2022. 2022. p. hal-03778289.
[10] Kausika BB, Nijmeijer D, Reimerink I, Brouwer P, Liem V. GeoAI for detection of solar photovoltaic installations in the Netherlands. Energy AI 2021;6:100111. https://doi.org/10.1016/j.egyai.2021.100111.
[11] SolarPower Europe. Global market outlook for solar power — 2021–2025. 2021.
[12] International Energy Agency (IEA). World Energy Outlook 2020. 2020.
[13] Mordor Intelligence. Global solar thermal market (2022–2027). 2022.
[14] Ren S, Hu W, Bradbury K, Harrison-Atlas D, Malaguzzi Valeri L, Murray B, et al. Automated extraction of energy systems information from remotely sensed data: a review and analysis. Appl Energy 2022;326:119876. https://doi.org/10.1016/j.apenergy.2022.119876.
[15] Yu J, Wang Z, Majumdar A, Rajagopal R. DeepSolar: A machine learning framework to efficiently construct a solar deployment database in the United States. Joule 2018;2:2605–17. https://doi.org/10.1016/j.joule.2018.11.021.
[16] Hou X, Wang B, Hu W, Yin L, Wu H. SolarNet: a deep learning framework to map solar power plants in China from satellite imagery. ICLR 2020 Workshop on Tackling Climate Change with Machine Learning. 2020.
[17] Kruitwagen L, Story KT, Friedrich J, Byers L, Skillman S, Hepburn C. A global inventory of photovoltaic solar energy generating units. Nature 2021;598:604–10. https://doi.org/10.1038/s41586-021-03957-7.
[18] Yuan J, Yang HHL, Omitaomu OA, Bhaduri BL. Large-scale solar panel mapping from aerial images using deep convolutional networks. In: 2016 IEEE International Conference on Big Data, Big Data 2016. IEEE; 2016. p. 2703–8. https://doi.org/10.1109/BigData.2016.7840915.
[19] Malof JM, Li B, Huang B, Bradbury K, Stretslov A. Mapping solar array location, size, and capacity using deep learning and overhead imagery. ArXiv 2019. abs/1902.1.
[20] Hu W, Bradbury K, Malof JM, Li B, Huang B, Streltsov A, et al. What you get is not always what you see—pitfalls in solar array assessment using overhead imagery. Appl Energy 2022;327:120143. https://doi.org/10.1016/j.apenergy.2022.120143.
[21] Rausch B, Mayer K, Arlt M-L, Gust G, Staudt P, Weinhardt C, et al. An enriched automated PV registry: combining image recognition and 3D building data. ArXiv 2020.
[22] Mayer K, Rausch B, Arlt ML, Gust G, Wang Z, Neumann D, et al. 3D-PV-Locator: Large-scale detection of rooftop-mounted photovoltaic systems in 3D. Appl Energy 2022;310:118469. https://doi.org/10.1016/j.apenergy.2021.118469.
[23] Wang Z, Arlt M-L, Zanocco C, Majumdar A, Rajagopal R. DeepSolar++: Understanding residential solar adoption trajectories with computer vision and technology diffusion models. Joule 2022:1–15. https://doi.org/10.1016/j.joule.2022.09.011.
[24] Lindahl J, Ekbring S, Johansson R, Lingfors D, Munkhammar J. Socioeconomic and demographic factors behind the deployment of domestic photovoltaic and solar thermal systmes in three Swedish municipalities. In: 8th World Conference on Photovoltaic Energy Conversion; 2022. p. 1530–40. https://doi.org/10.4229/WCPEC-82022-5DO.10.5.
[25] Xia Z, Li Y, Chen R, Sengupta D, Guo X, Xiong B, et al. Mapping the rapid development of photovoltaic power stations in northwestern China using remote sensing. Energy Rep 2022;8:4117–27. https://doi.org/10.1016/j.egyr.2022.03.039.
[26] Bradbury K, Saboo R, Johnson TL, Malof JM, Devarajan A, Zhang W, et al. Distributed solar photovoltaic array location and extent dataset for remote sensing object identification. Sci Data 2016;3:1–9. https://doi.org/10.1038/sdata.2016.106.
[27] Kasmi G, Saint-Drenan Y-M, Trebosc D, el Jolivet R, Leloux J, Sarr B, et al. A crowdsourced dataset of aerial images with annotated solar photovoltaic arrays and installation metadata, 2022, p. 1–12.
[28] Castello R, Roquette S, Esguerra M, Guerra A, Scartezzini JL. Deep learning in the built environment: automatic detection of rooftop solar panels using convolutional neural networks. J Phys Conf Ser 2019;1343:1–6. https://doi.org/10.1088/1742-6596/1343/1/012034.
[29] Mayer K, Wang Z, Arlt ML, Neumann D, Rajagopal R. DeepSolar for Germany: a deep learning framework for PV system mapping from aerial imagery. In: Proceedings of the 3rd International Conference on Smart Energy Systems and Technologies (SEST); 2020. p. 11–6. https://doi.org/10.1109/SEST48500.2020.9203258.
[30] Costa MVCV da, Carvalho OLF de, Orlandi AG, Hirata I, Albuquerque AO de, Silva FV e, et al. Remote sensing for monitoring photovoltaic solar plants in brazil using deep semantic segmentation. Energies (Basel) 2021;14:1–15. https://doi.org/10.3390/en14102960.
[31] Zhang X, Zeraatpisheh M, Rahman MM, Wang S, Xu M. Texture is important in improving the accuracy of mapping photovoltaic power plants: a case study of Ningxia autonomous region, China. Remote Sens (Basel) 2021;13. https://doi.org/10.3390/rs13193909.
[32] Malof JM, Collins LM, Bradbury K. A deep convolutional neural network, with pre-training, for solar photovoltaic array detection in aerial imagery. In: International Geoscience and Remote Sensing Symposium (IGARSS) 2017; 2017. p. 874–7. https://doi.org/10.1109/IGARSS.2017.8127092.
[33] Lindahl J, Oller Westerberg A. National Survey Report of PV Power Applications in Sweden 2021. 2022.

[34] Energimyndigheten. Nätanslutna solcellsanläggningar 2021. https://www.energimyndigheten.se/statistik/den-officiella-statistiken/statistikprodukter/natanslutna-solcellsanlaggningar/n/statistikprodukter/natanslutna-solcellsanlaggningar/ (accessed April 8, 2021).
[35] Energimyndigheten. Solvärme i Sverige — En studie med fokus på potential, ekonomi och bidrag till energi- och klimatmål. 2021.
[36] Boverket. Utvärdering av solvärmebidraget och solvärmestödet. 2012. Karlskrona.
[37] Louvet Y, Fischer S, Furbo S, Giovannetti F, Helbig S, Köhl M, et al. Economic comparison of reference solar thermal systems for households in five European countries. Solar Energy 2019;193:85–94. https://doi.org/10.1016/j.solener.2019.09.019.
[38] Bankel A, Mignon I. Solar business models from a firm perspective – an empirical study of the Swedish market. Energy Policy 2022;166:113013. https://doi.org/10.1016/j.enpol.2022.113013.
[39] Lindahl J, Lingfors D, Å Elmqvist, Mignon I. Economic analysis of the early market of centralized photovoltaic parks in Sweden. Renew Energy 2022;185:1192–208. https://doi.org/10.1016/j.renene.2021.12.081.
[40] Li P, Zhang H, Guo Z, Lyu S, Chen J, Li W, et al. Understanding rooftop PV panel semantic segmentation of satellite and aerial images for better using machine learning. Adv Appl Energy 2021;4:100057. https://doi.org/10.1016/j.adapen.2021.100057.
[41] Frimane Å, Johansson R, Munkhammar J, Lingfors D, Lindahl J. Identifying small decentralized solar systems in aerial images using deep learning. Solar Energy 2023;262. https://doi.org/10.1016/j.solener.2023.111822.
[42] Woersdorfer JS, Kaus W. Will nonowners follow pioneer consumers in the adoption of solar thermal systems? Empirical evidence for northwestern Germany. Ecol Econ 2011;70:2282–91. https://doi.org/10.1016/j.ecolecon.2011.04.005.
[43] Huang J, Tian Z, Fan J. A comprehensive analysis on development and transition of the solar thermal market in China with more than 70% market share worldwide. Energy 2019;174:611–24. https://doi.org/10.1016/j.energy.2019.02.165.
[44] Hirvonen J, ur Rehman H, Sirén K. Techno-economic optimization and analysis of a high latitude solar district heating system with seasonal storage, considering different community sizes. Solar Energy 2018;162:472–88. https://doi.org/10.1016/j.solener.2018.01.052.
[45] Tschopp D, Tian Z, Berberich M, Fan J, Perers B, Furbo S. Large-scale solar thermal systems in leading countries: a review and comparative study of Denmark, China, Germany and Austria. Appl Energy 2020;270:114997. https://doi.org/10.1016/j.apenergy.2020.114997.
[46] Tian Z, Zhang S, Deng J, Fan J, Huang J, Kong W, et al. Large-scale solar district heating plants in Danish smart thermal grid: Developments and recent trends. Energy Convers Manag 2019;189:67–80. https://doi.org/10.1016/j.enconman.2019.03.071.